Bioactive Materials 15 (2022) 272–287

Contents lists available at ScienceDirect

Bioactive Materials

journal homepage: www.keaipublishing.com/en/journals/bioactive-materials

Acellular nerve grafts supplemented with induced pluripotent stem cell-derived exosomes promote peripheral nerve reconstruction and motor function recovery

Jianfeng Pan [a], Meng Zhao [b], Xiangjiao Yi [c], Jianguo Tao [b], Shaobo Li [b], Zengxin Jiang [d,e], Biao Cheng [a], Hengfeng Yuan [d,e,*], Feng Zhang [f,**]

[a] Department of Orthopedics, Shanghai Tenth People's Hospital, School of Medicine, Tongji University, Shanghai, 200072, China
[b] Diseases & Population Geninfo Lab, School of Life Sciences, Westlake University, Hangzhou, Zhejiang, 310024, China
[c] Institute of Orthopaedics and Traumatology, Zhejiang Chinese Medical University Affiliated First Affiliated Hospital, Hangzhou, Zhejiang, 310024, China
[d] Department of Orthopaedics, Shanghai Jiaotong University Affiliated Sixth People's Hospital, Shanghai, 200233, China
[e] Institute of Microsurgery On Extremities, Shanghai Jiao Tong University Affiliated Sixth People's Hospital, Shanghai, 200233, China
[f] Joseph M. Still Burn and Reconstructive Center, Jackson, MS, 39204, USA

ARTICLE INFO

Keywords:
Induced pluripotent stem cells
Exosomes
Acellular nerve grafts
Peripheral nerve reconstruction
Motor function recovery

ABSTRACT

Peripheral nerve injury is a great challenge in clinical work due to the restricted repair gap and weak regrowth ability. Herein, we selected induced pluripotent stem cells (iPSCs) derived exosomes to supplement acellular nerve grafts (ANGs) with the aim of restoring long-distance peripheral nerve defects. Human fibroblasts were reprogrammed into iPSCs through non-integrating transduction of Oct3/4, Sox2, Klf4, and c-Myc. The obtained iPSCs had highly active alkaline phosphatase expression and expressed Oct4, SSEA4, Nanog, Sox2, which also differentiated into all three germ layers in vivo and differentiated into mature peripheral neurons and Schwann cells (SCs) in vitro. After isolation and biological characteristics of iPSCs-derived exosomes, we found that numerous PKH26-labeled exosomes were internalized inside SCs through endocytotic pathway and exhibited a proliferative effect on SCs that were involved in the process of axonal regeneration and remyelination. After that, we prepared ANGs via optimized chemical extracted process to bridge 15 mm long-distance peripheral nerve gaps in rats. Owing to the promotion of iPSCs-derived exosomes, satisfactory regenerative outcomes were achieved including gait behavior analysis, electrophysiological assessment, and morphological analysis of regenerated nerves. Especially, motor function was restored with comparable to those achieved with nerve autografts and there were no significant differences in the fiber diameter and area of reinnervated muscle fibers. Taken together, our combined use of iPSCs-derived exosomes with ANGs demonstrates good promise to restore long-distance peripheral nerve defects, and thus represents a cell-free strategy for future clinical applications.

1. Introduction

Peripheral nerve injury is a common clinical problem, which often leads to loss of motor function, sensory disturbance and neuropathic pain in the innervated area [1–4]. Among various types of peripheral nerve injuries, complete transection usually causes long-distance nerve defects that may have a devastating impact on the life quality of patients. The treatment for peripheral nerve defects continues to be a significant clinical challenge, although reconstructive surgery is considered as a therapeutic strategy to promote nerve regeneration and functional recovery. In most cases, nerve grafts are required as a bridge to span peripheral nerve gap between the proximal and distal nerve stumps. The typical choice is autologous nerve grafts, which usually are the nonsignificant nerve segments from the patient's non-functional area, such as sural nerve and superficial cutaneous nerve grafts [5,6]. The autologous nerve transplantation is the most effective surgical method for the treatment of peripheral nerve defects, and it is also the "gold standard" to evaluate the effectiveness of other nerve

Peer review under responsibility of KeAi Communications Co., Ltd.
* Corresponding author. Department of Orthopaedics, Shanghai Jiaotong University Affiliated Sixth People's Hospital, Shanghai, 200233, China.
** Corresponding author.
E-mail addresses: yuanhf@shsmu.edu.cn (H. Yuan), feng.zhang@burncenters.com (F. Zhang).

https://doi.org/10.1016/j.bioactmat.2021.12.004
Received 22 September 2021; Received in revised form 5 December 2021; Accepted 10 December 2021
Available online 20 December 2021

reconstruction strategies [7–9]. However, the use of autologous nerve grafts is limited by the inherent drawbacks, such as limited nerve tissue availability, second surgery to obtain autologous nerve, potential mismatch between injured nerve and donor nerve, as well as donor-site morbidities and deformities. Therefore, promising alternative strategies to autologous nerve grafts need to be developed for peripheral nerve reconstruction and functional restoration.

As alternatives to autologous nerve grafts, autologous non-neural tissues and allogeneic or xenogeneic nerve grafts have been used as nerve scaffolds to bridge peripheral nerve gaps. Non-neural tissues have been demonstrated to get very limited success in promoting peripheral nerve regeneration, including muscles, veins, tendons, and epineurial sheaths [10]. After grafting nerve gaps with allogeneic nerve grafts, the outcomes of peripheral nerve regeneration are also not all satisfactory. The types of donor nerve play a crucial role in the ultimate results of functional restoration, especially for the recovery of critical motor function. Compared with sensory nerve grafts, the use of motor or mixed nerve grafts optimized axonal regeneration with superior outcomes in nerve gap model [11,12]. This suggests that motor nerve tissues harvested from allogeneic or xenogeneic species can be employed as ideal sources for preparing nerve scaffolds.

Due to the inevitable immune responses, allogeneic nerve grafts necessitate to remove the immunogenic components before they are implanted in vivo. A variety of methods have been developed to remove immunogenic constituents including physical, chemical and enzymatic treatments. The basal lamina tubes in native nerve architecture are essential for guiding regenerating axons to their denervated targets. In the process of decellularization, the satisfactory goal is to efficiently remove all immunogenic materials while retaining the internal structure of natural nerves. Compared with the predominant current protocols, optimized chemical process presented an improved acellular nerve graft that removed cellular materials and preserved the integrity of basal lamina tubes to support nerve regeneration [13,14].

Since the decellularization process is dedicated to removing immunogenic cells and retaining extracellular matrix (ECM) components that are basically conserved among species, the resulting acellular nerve grafts (ANGs) can be used as a very suitable substitute for autologous nerve grafts to bridge peripheral nerve defects. However, the use of ANGs alone to restore peripheral nerve defects can only be effective in the reconstruction of small peripheral nerve gaps (rat sciatic nerve <10 mm or primate ulnar nerve <30 mm) [15]. When the length of nerve gaps exceeds the limitations, the therapeutic effects of ANGs become less satisfactory [16]. Supplementing ANGs with cells-based or regenerative environmental strategies can improve the increasing length of nerve defects [17].

One of the choices is stem cells that have attracted considerable interest for their potential applicability in peripheral nerve regeneration. Stem cells create a favorable environment to regenerate damaged nerve axons and facilitate functional recovery. Embryonic stem cells (ESCs), induced pluripotent stem cells (iPSCs), mesenchymal stem cells (MSCs) derived from adipose tissue, bone marrow, synovium and periosteum have shown various therapeutic effects on peripheral nerve system. In the past, stem cells were considered to accelerate tissue regeneration mainly through their proliferative capacity and multipotent differentiation ability. However, their use is still restricted due to relatively cumbersome differentiative protocols and methodological limitations. Moreover, the frequency of engraftment and transdifferentiation after stem cell transplantation to produce new target cells seems too low to explain the observed beneficial effects [18]. Increasing evidences have proposed that stem cells participate in the processes of tissue repair through an indirect pathway of paracrine mechanism. Direct support comes from Bi's study demonstrating that the administration of conditioned medium from stem cells mimics the beneficial effects of stem cell therapy [19]. If cell-free strategies can completely replace stem cells to promote nerve regeneration, they will be the simplest strategies to treat peripheral nerve defects. In the process of regeneration stimulated by stem cells, the involved paracrine mediators may include not only soluble bioactive molecules, but also exosomes released from stem cells.

Exosomes are one of the extracellular vesicles secreted by cells, which contain numerous proteins, lipids and nucleic acids for cell-to-cell communication. The horizontal transfer of exosomes between cells results in incorporating messenger RNAs (mRNAs) to encode "obtained" proteins [20,21] or micro RNAs (miRNAs) to inhibit "inherent" mRNA translation in recipient cells [22,23], and subsequently influence the physiological behavior to favor tissue regeneration [24]. It has been reported that exosomes have similar functions to parent cells of their origin [25]. By replacing stem cells with exosomes in transplantation, many safety issues and limitations related to stem cells can be resolved. The use of exosomal therapy bypasses the biological safety issues of stem cell therapy, does not involve implantation of living cells into the body, and does not have the risk of cell proliferation or mutation. Compared with exogenous cells, exosomes have the advantages of non-immunogenicity, convenient storage, and stable biochemical activities. Exosomes can be stored at −70 °C for several months without any change in their biological effects [26]. Moreover, the rationale for exosomes in tissue regeneration is proposed that the administration of exosomes at the site of tissue injury may induce de-differentiation of resident cells, re-entry to cell cycle and activation of tissue regenerative procedures [27].

Hence, the use of exosomes to supplement ANGs is a valuable strategy to improve the treatment of long-distance peripheral nerve defects. The application of human iPSCs-derived exosomes has not been reported till now to promote peripheral nerve regeneration. IPSCs were firstly established from adult fibroblasts by Yamanaka with the advantage of avoiding complicated ethical concerns associated with ESCs [28]. Human iPSCs were similar to human ESCs in morphology, growth properties, surface markers, pluripotent cell-specific gene expression, telomerase activities and differentiation [29]. The unlimited expansion potential of iPSCs further makes them an ideal parent cell for generating stable amounts of exosomes while MSCs tend to become senescent that results in cell proliferation arrest during ex vivo expansion [30].

In the present study, we firstly used the optimized chemical process to produce ANGs from motor nerve tissues of Sprague-Dawley (SD) rats. Then we established human iPSCs from adult human dermal fibroblasts by the transduction of four reprogramming factors Oct3/4, Sox2, Klf4, and c-Myc. With the aim of establishing a cell-free strategy for the reconstruction of long-distance peripheral nerve defects, we examined the therapeutic potential of human iPSCs-derived exosomes by transplanting them with ANGs to bridge a 15 mm long-distance gap created in the sciatic nerve of SD rats.

2. Materials and methods

2.1. Generation and characterization of iPSCs from human fibroblasts

The study was approved by the ethics committee of Tongji University Affiliated Tenth People's Hospital (SHDSYY-2017-4427). The fibroblast culture was derived from skin tissue of the donor. CytoTune®-iPS 2.0 Sendai Reprogramming Kit (Life Technology) was used to reprogram fibroblasts into iPSCs according to the manufacturer's instructions. After transduction, iPSCs colonies were cultured on tissue dishes coated with Matrigel using mTeSR-1 medium. Immunofluorescence and alkaline phosphatase (ALP) staining was performed to characterize reprogramed iPSCs. Following fixation with 4% paraformaldehyde solution for 15 min, iPSCs were permeabilized with 0.2% Triton X-100 for 15 min and blocked with 1% BSA for 2 h. Primary antibodies (including Oct4, SSEA4, Nanog and Sox2) were applied to incubate iPSCs at 4 °C overnight and secondary antibodies were applied for 1 h, followed by Nuclei counterstain with 4,6-diamidino-2-phenylindole (DAPI). ALP staining was conducted using ALP Detection Kit after fixed with 4% paraformaldehyde solution following the manufacturer's instructions.

2.2. In vitro differentiation and in vivo teratoma formation

For embryoid body (EB) formation, iPSCs were dispersed into small cell clumps and cultured in suspension for 7 days to get EBs. To initiate differentiation, the formed EBs were then cultured in 0.1% gelatin-coated plates in neural crest (NC) induction medium containing Stem-Pro Neural Supplement, KnockOut DMEM/F-12, 1% Glutamax, 20 ng/ml bFGF and 10 ng/ml EGF for 10 days. The colonies with rosette structures were harvested and the markers for neural crest stem cells (NCSCs) were analyzed by immunofluorescence assay. For Schwann cell differentiation, NCSCs were transferred and cultured in Neurobasal medium supplemented with ciliary neurotropic factor (CNTF, 10 ng/ml), neuregulin 1β (20 ng/ml) and dibutyryl cyclic AMP (dbcAMP, 1 mM) for 3 weeks. For neuronal differentiation, NCSCs were transferred and cultured in Neurobasal medium supplemented with B27, brain-derived neurotrophic factor (BDNF, 10 ng/ml), glial cell line-derived neurotrophic factor (GDNF, 10 ng/ml), nerve growth factor (NGF, 10 ng/ml), and dbcAMP (1 mM) for 3 weeks. For teratomas formation, iPSCs was dispersed into Matrigel at the density of 1×10^7 cells/ml and A total of 100 μl (1×10^6 cells) were injected subcutaneously into the dorsal flank of NOD/SCID mice. After 8 weeks, the teratoma was surgically harvested from the mice. All samples were fixed in para-formaldehyde and embedded in paraffin. Sections were stained with hematoxylin and eosin (H&E).

2.3. Isolation and biological characteristics of exosomes from iPSCs

When iPSCs reached 80–90% confluence, the conditioned medium was collected and further processed with sequential centrifugation to prepare exosomes. Firstly, the supernatants were centrifuged at 500×*g* for 10 min to remove the floating cells. After that, the supernatants were centrifuged at 10,000×*g* for 30 min at 4 °C to remove cell debris and apoptotic bodies. Then the supernatants were centrifuged at 100,000×*g* at 4 °C for 70 min to precipitate exosomes. IPSCs-derived exosomes were resuspended in PBS and stored at −80 °C for further analysis. The protein concentration was determined with the BCA protein assay. The morphology of iPSCs-derived exosomes was observed by transmission electron microscopy. Size distribution and concentration was analyzed using NanoSight NS500 instrument equipped with particle-tracking video capture. After characterization, iPSCs-derived exosomes were isolated from blue fluorescent carbon dot-loaded iPSCs to label their content. The exosomal membrane was labeled with red fluorescent marker DiI and incubated with SCs that were labeled with green membrane fluorescent marker DiO to visualize transfer of their content and internalization of iPSCs-derived exosomes to recipient cells. Then, the effect of iPSCs-derived exosomes on the proliferation of SCs was evaluated by CCK-8 assay and flow cytometry analysis. In the CCK-8 assay, no exosomes treatment served as control group. In the flow cytometry analysis, SCs-derived exosomes were prepared and compared with iPSCs-derived exosomes to analyze if the effect is specifically linked to iPSC exosomes.

2.4. Construction and evaluation of acellular nerve grafts with optimized chemical extracted process

Acellular nerve grafts were fabricated following the protocol of optimized chemical extracted process. Firstly, the sciatic nerves were harvested from both sides of rats under aseptic conditions and cut into 15 mm segments. The washing solution A contained 10 mM phosphate and 50 mM sodium. The chemical solution A contained 125 mM sulfobetaine-10 (SB-10), 10 mM phosphate and 50 mM sodium. The chemical solution B contained 0.14% Triton X-200, 0.6 mM sulfobetaine-16 (SB-16), 10 mM phosphate and 50 mM sodium. The washing solution B contained 50 mM phosphate and 100 mM sodium. The nerves were washed in deionized distilled water at 25 °C with agitation for 7 h. Then the nerves were agitated in chemical solution A for 15 h and rinsed in washing solution B for 15 min. After that, the nerves were agitated in chemical solution B for 24 h and rinsed in washing solution B three times (5 min each). Next, the nerves were agitated in chemical solution A for 7 h, rinsed in washing solution B for 15 min, and agitated in chemical solution B for 15 h. At last, the nerve grafts were rinsed in washing solution A three times (15 min each) and stored in washing solution A at 4 °C.To evaluate cellular removal and ECM preservation after optimized chemical extracted process, acellular nerve grafts were compared with fresh nerve tissue including scanning electron microscopy (SEM), Protein electrophoresis analysis and immunofluorescence staining.

2.5. In vivo transplantation to promote sciatic nerve regeneration

Adult SD rats weighing 300–350 g were divided into three groups: (1) autograft group bridged with autologous nerve grafts; (2) acellular nerve allograft (ANA) group bridged with acellular nerve grafts and (3) iPSCs-derived exosomes group bridged with acellular nerve grafts and iPSCs-derived exosomes (ANA + iPSCs-exosomes). The sciatic nerve was excised and removed, creating a long-distance nerve gap of 15-mm between the two stumps. The corresponding nerve grafts were implanted across the nerve defects and sutured with 10-0 sutures under microscope.

1) Walking track analysis and electrophysiology

At 1, 2, 4, 8, and 12 weeks after surgery, walking track analysis and electrophysiological tests were performed to assess the regeneration of the sciatic nerve across the defects (n = 5 at each time point). The hind paws were dipped with nontoxic ink and the rats were allowed to walk down a trace to record their paw prints. Five footprints were taken to calculate the sciatic functional index (SFI) as follows: SFI = 109.5 × TSF + 13.3 × ITF -38.3 × PLF - 8.8, where toe spread factor TSF = (ETS-NTS)/NTS, intermediate toe spread factor ITF = (EIT-NIT)/NIT, and print length factor (PLF) = (EPL-NPL)/NPL. Print length (PL) is the distance from the heel to the third toe; toe spread (TS) is the distance from the first toe to the fifth toe; intermediary toe spread (IT) is the distance from the second toe to the fourth toe; E represents the experimental side, and N represents the unoperated side.

After anesthesia, electrical stimulation (0.5 mA, 0.2 ms, 0.5Hz) was applied to the sciatic nerve trunk 5 mm proximal to the implant site. The electrodes were inserted in the belly of gastrocnemius and anterior tibialis muscles to record compound muscle action potentials (CMAPs). The CMAP latency and CMAP maximum amplitude were recorded for each muscle. For comparison, normal CMAPs were recorded at the nonoperative contralateral side. The nerve conduction velocity (NCV), CMAP latency and amplitude recovery index (RI) of CMAPs were calculated.

2) Histological analysis and evaluation of myelination

After electrophysiological assessment, the regenerative nerve was harvested and fixed in 2.5% glutaraldehyde at 4 °C for 24 h. The sample was subsequently fixed in 1% osmium tetroxide for 2 h and embedded in resin. The middle portion of the explanted grafts was sectioned in transverse semithin to stain with 1% toluidine blue. The cross-sectional area of myelinated axons, the diameter of myelinated axons, and the number of myelinated axons per unit area was quantified by using ImageJ software (NIH, USA).

2.6. Histological and functional analysis of the reinnervated muscles by the regenerated nerve

At each time point, the reinnervated muscles were analyzed including muscle strength testing, muscle weight measurement and histological morphometry. After anesthesia, bilateral gastrocnemius and

anterior tibialis muscles were isolated and connected to a tension transducer (JZJ101, Chengdu Instrument Factory, China). 0.2 ms electrical stimuli of three different voltages were applied on each muscle to get the maximum force under physiological muscle stretch. The muscle maximum tension recovery ratio (MTRR) was calculated as the tetanic tension ratio of experimental to nonoperative side. Then target muscles on experimental and nonoperative sides were harvested and weighed to calculate the muscle weight maintaining ratio (MWMR) as the weight ratio of experimental to nonoperative side. The harvested muscles were fixed in paraformaldehyde and embedded in paraffin. Sections were stained with H&E and examined under light microscope.

2.7. Statistical analysis

All experiments unless mentioned were repeated at least three times. Differences among different groups were evaluated by one-way ANOVA test, and the differences from the same group were analyzed by the Student's t-test via SPSS 17.0 software (SPSS, USA). The data were expressed as the mean ± standard deviation (SD) and differences were considered statistically significant when p values < 0.05.

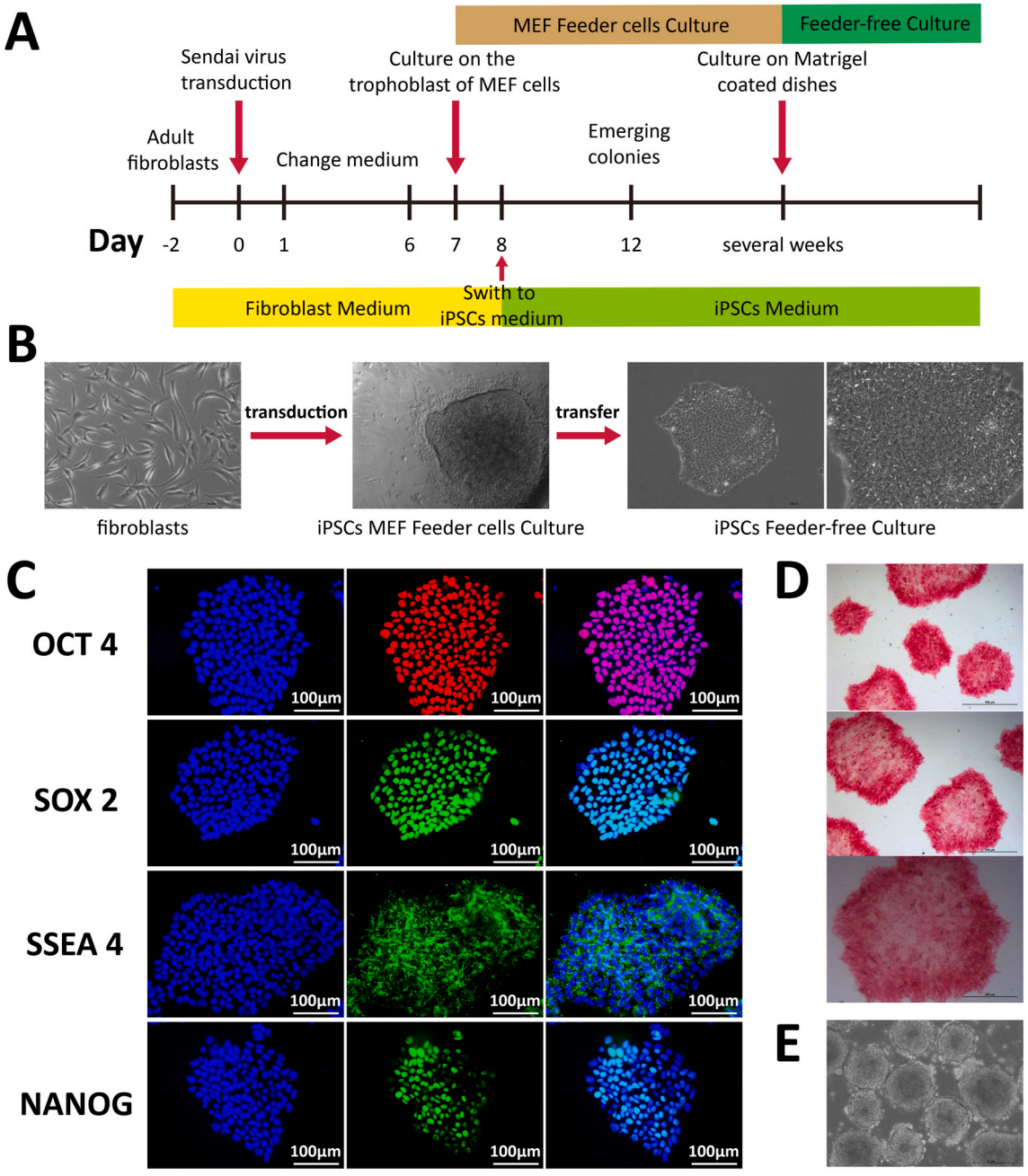

Fig. 1. Generation and characterization of iPSCs derived from human fibroblasts. (A) The scheme of the reprogramming procedures of fibroblasts. (B) The morphology of human fibroblasts, iPSCs cultured on the trophoblast of MEF cells, and iPSCs cultured on feeder-free dishes. (C) Immunofluorescent staining showed that human iPSCs showed similar morphology to embryonic stem cells and were positive for OCT4, SOX2, SSEA4 and NANOG. Nuclei were stained with 4′,6-Diamidin-2-phenylindol (DAPI). (D) Human iPSCs were positive for alkaline phosphatase. (E) In vitro embryoid body formation and differentiation.

3. Results

3.1. Generation and characterization of iPSCs from human fibroblasts

The protocol for reprogramming fibroblasts was depicted in Fig. 1A. We introduced non-integrating Sendai virus vectors containing human Oct3/4, Sox2, Klf4, and c-Myc to reprogram adult fibroblasts into iPSCs. The primary cultured human skin fibroblasts showed a certain proliferative and expansive capacity. After 2–3 passages, the obtained fibroblasts exhibited long fusiform and polygonal appearance with uniform cell morphology (Fig. 1B). After Sendai virus infection, it was observed that fibroblasts became smaller, changing from a long spindle to a round shape, and the cells were clustered under light microscope. On the trophoblast of MEF cells, cell growth presented a multi-layered colony-like state, similar to cell clones of embryonic stem cells. The cell colonies gradually expanded with the increase of culture time. Then the induced cells were seeded and cultured in a culture plate coated with Matrigel. The iPSCs propagated well adherently with uniform morphology and round shape. High nuclear-to-cytoplasmic ratio was detected with larger nuclei, larger nucleoli and relatively less cytoplasm (Fig. 1B). In the proliferative process of iPSCs, they were clustered together and tightly arranged without obvious cell boundaries. Cell clones were island-like with clear edges. The iPSCs at the center and the edges of clone were uniform and identical.

After complete reprogramming of somatic cells, iPSCs expressed a series of pluripotency-related genes and form a pluripotency regulatory network similar to embryonic stem cells. These gene products included Oct4, SSEA4, Nanog and Sox2. Immunofluorescence staining revealed that iPSCs induced by human fibroblasts positively expressed octamer binding protein OCT-4, specific stage embryonic antigen SSEA4, nucleoprotein Nanog, and Sox2 (Fig. 1C). It was preliminarily confirmed that iPSCs showed the specific expression of pluripotency-related genes and possessed the potential for stemness and downstream differentiation at the molecular level.

When iPSCs reached about 50% confluence, we analyzed ALP activity of generated iPSCs to examine the undifferentiated status of each iPSCs colony. ALP is one of the identification indicators of iPSCs. As shown in Fig. 1D, the colonies of iPSCs were positively stained by ALP. Strong ALP activity was observed to stain as positive red. The expression of ALP activity was activated during the induction of somatic cells into iPSCs. The undifferentiated status of iPSCs was characterized by high level of expression of ALP activity. After differentiation, ALP expression was decreased. It was seen that each iPSCs clone was evenly stained by ALP, and the iPSCs in the clone were all positively expressing ALP.

As shown in Fig. 1E, iPSCs aggregated into cell spheres of varying sizes in suspension culture. After a period of incubation, the cell spheres extended in volume and gradually formed embryoid somatic cell spheres. With the time of culture in vitro, EB cell spheres further

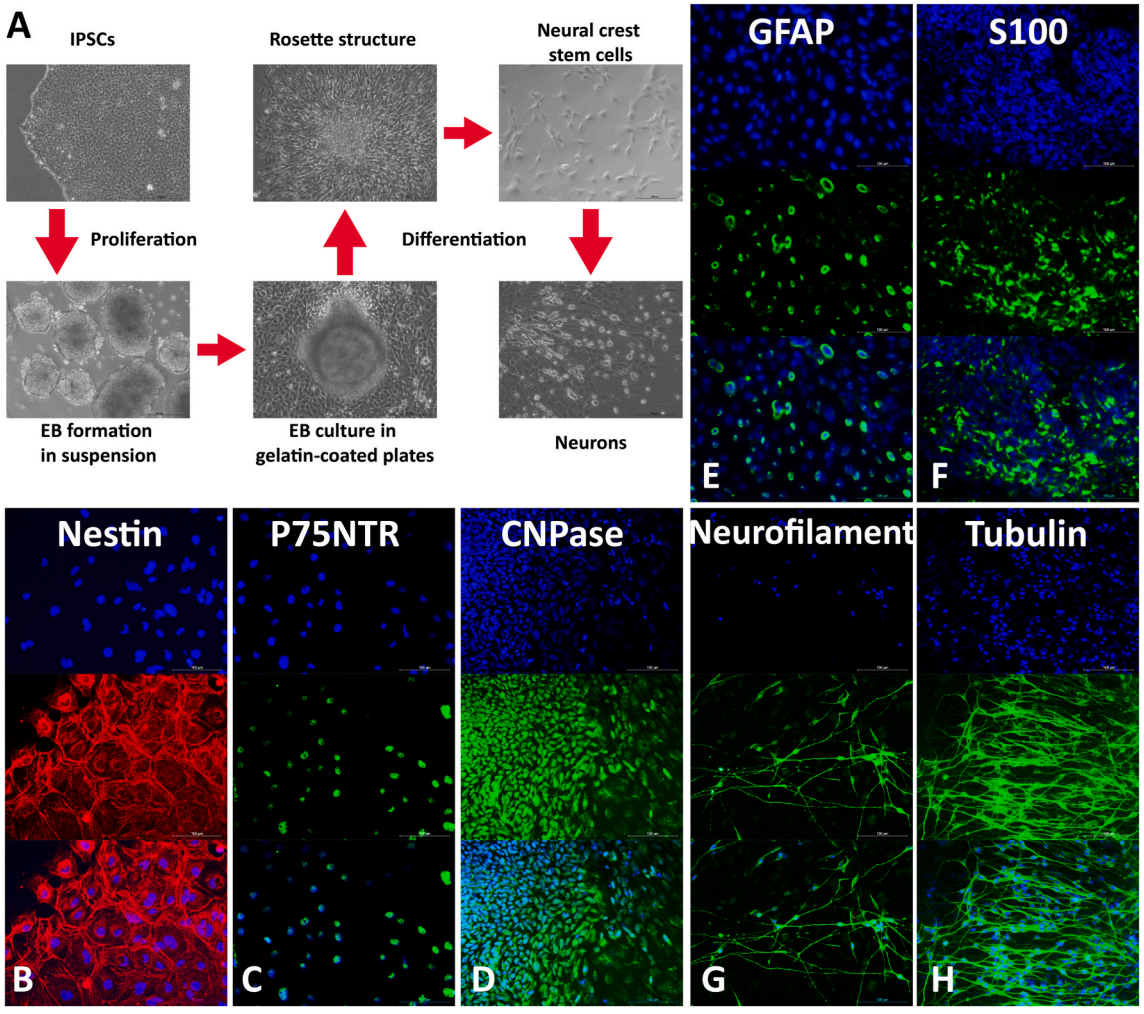

Fig. 2. Expansion and neural differentiation potential of iPSCs. (A) The procedure to differentiate iPSCs into neural crest stem cells (NCSCs) and mature neural cells. Cell colonies with rosette structures were positive for neural crest markers Nestin (B), p75NTR (C) and CNPase (D). After neural differentiation process, iPSCs differentiated into peripheral neural cells positive for Schwann cell markers GFAP (E) and S100 (F). The immunofluorescent staining showed that iPSCs differentiated into mature peripheral neurons positive for the axon marker neurofilament (G) and tubulin (H). Nuclei were stained with DAPI.

extended and there was a tendency to differentiate into other cells.

3.2. Expansion and neural differentiation potential of iPSCs

We differentiated iPSCs into neural cell lineages as described in Fig. 2A. Human iPSCs were first cultured as cell aggregates in suspension to form EBs. The EBs were cultured in gelatin-coated plates allowing cell adhesion to form rosette structures (Fig. 2A). At the rosette stage of iPSCs differentiation, NCSCs were isolated and positive for neural crest markers Nestin (Fig. 2B), p75NTR (Fig. 2C) and CNPase (Fig. 2D). During the differentiation process, the expression of various neural crest markers significantly increased while the expression of pluripotency-related markers Oct4, SSEA4, Nanog and Sox2 decreased. NCSCs became more homogeneous and further differentiated into peripheral neural lineages including SCs and peripheral neurons. After the neural induction by CNTF, neuregulin 1β and dbcAMP, NCSCs differentiated into SCs that positive for Schwann cell markers GFAP (Fig. 2E) and S100 (Fig. 2F). Mature peripheral neurons were induced by the combination of BDNF, GDNF, NGF and dbcAMP, which were confirmed by immunostaining for the axon markers neurofilament (Fig. 2G) and tubulin (Fig. 2H).

Except for peripheral neural lineages, iPSCs were also capable to differentiate into the mesodermal and endodermal lineages. We evaluated the differentiation of iPSCs into all three embryonic germ layers in vivo. The iPSCs displayed an ability to form teratoma in NOD/SCID mice. After injection of iPSCs subcutaneously, teratoma was formed and gradually increased with time. At 8 weeks, the diameter of the tumor was about 1.5 cm (Fig. 3A). Through HE staining analysis, advanced derivatives of three embryonic germ layers were observed in tumor. There were chondrocytes (Fig. 3B), adipocytes (Fig. 3C) and muscle fiber cells (Fig. 3D) that derived from the mesoderm of early embryo. Goblet cells arranged in gland-like structures (Fig. 3E) were defined as epithelium with intestinal differentiation, which were derived from embryonic endoderm. Besides, neural tissues in teratoma (Fig. 3F) and neural differentiation in vitro confirmed the potential of ectodermal differentiation. These results demonstrate that the generated iPSCs have the capacity of differentiating into all three germ layers in vivo.

3.3. Isolation and biological characteristics of exosomes from iPSCs

The iPSCs-derived exosomes were isolated and purified from iPSCs conditioned medium via ultra centrifugation. The protein concentration of exosomes was determined to be 2.94 mg/ml by BCA method. As shown in Fig. 4A, the morphology of iPSCs-derived exosomes was observed under transmission electron microscope. The exosomes

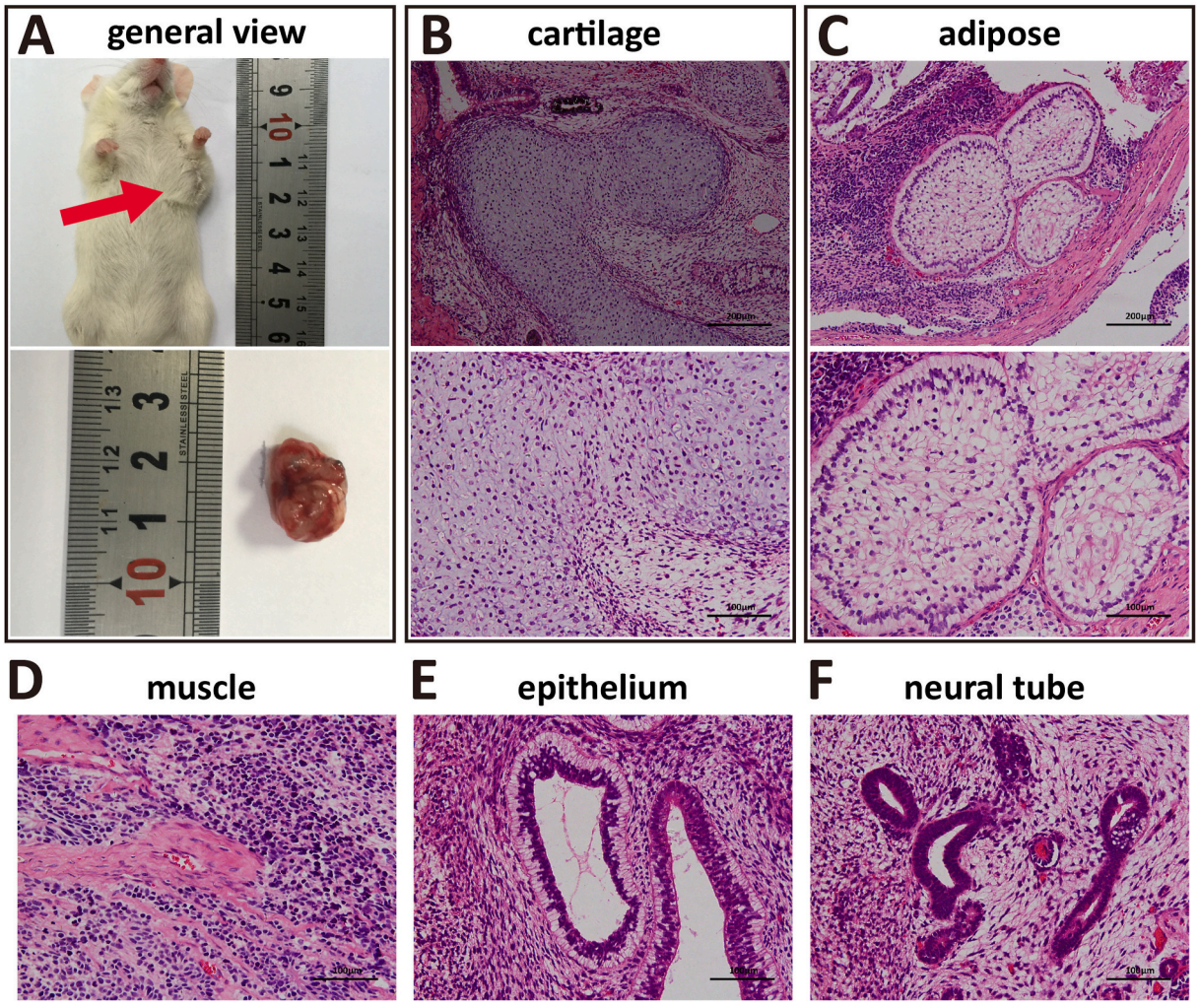

Fig. 3. Pluripotency of human iPSCs in vivo and H&E staining of teratoma. (A) IPSCs were injected subcutaneously in NOD/SCID mice and a tumor developed from the injection site. Various tissues were present in teratomas including cartilage (B), adipose tissue (C), muscle (D), gut-like epithelium (E), and neural tube-like tissues (F). Histology of the teratomas confirmed in vivo differentiation of iPSCs into all three germ layers (endoderm: epithelium; mesoderm: cartilage, adipose tissue, muscle; ectoderm: neural tissues). Scale bars, 100 mm.

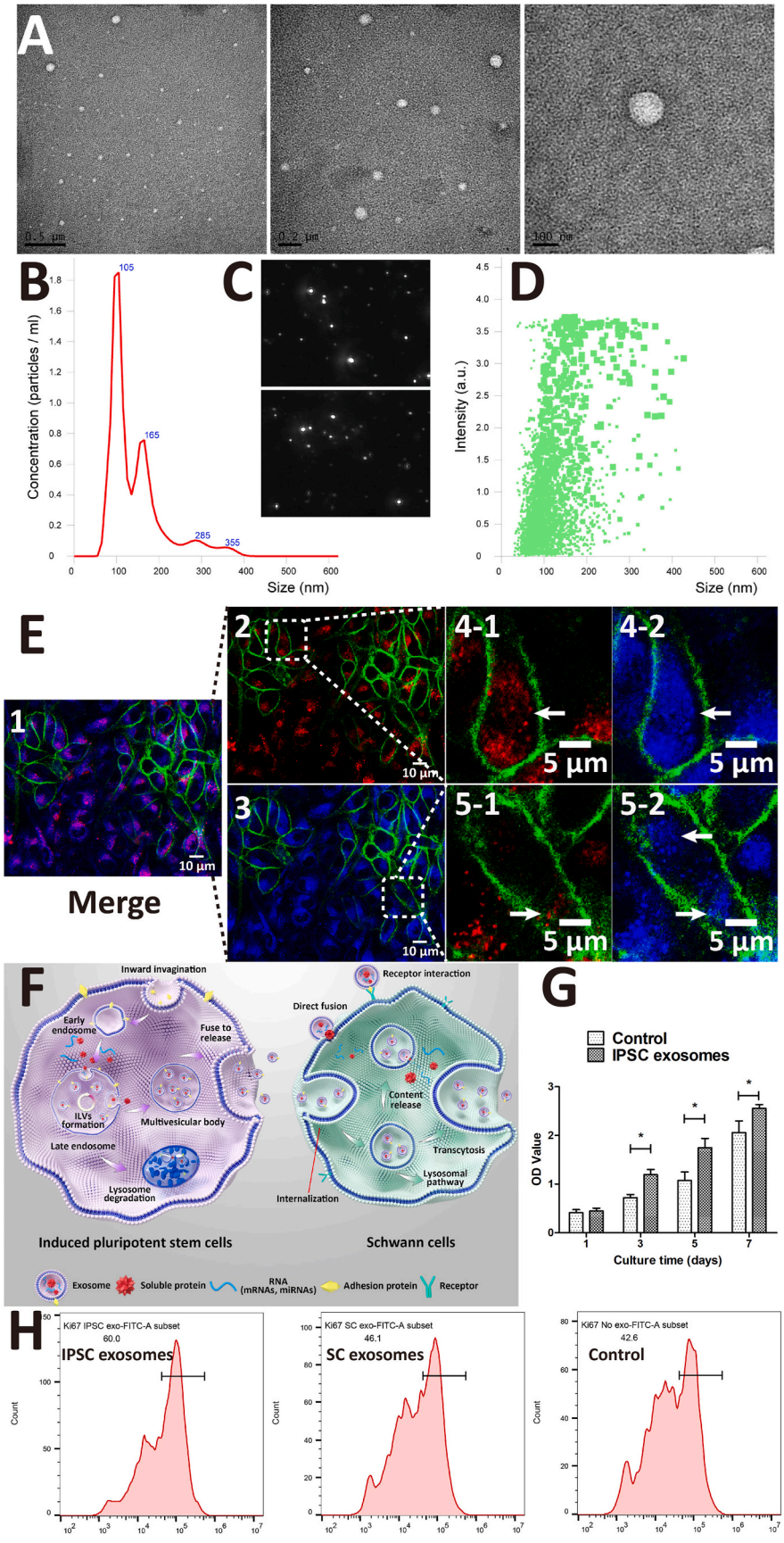

Fig. 4. Isolation and biological characteristics of exosomes from iPSCs. (A) The morphology of iPSCs-derived exosomes was observed under transmission electron microscope. (B) Diameter range and concentration of iPSCs-derived exosomes. (C) Nanoparticle tracking analysis of iPSCs-derived exosomes. (D) The distribution intensity of iPSCs-derived exosomes. (E) IPSCs-derived exosomes were internalized inside SCs through endocytotic pathway to release their content in the cytoplasm. (F) Schematic outline to show the internalization of iPSCs-derived exosomes by SCs through endocytosis mechanism. (G) IPSCs-derived exosomes promoted cell viability and proliferation of SCs after internalization process. Error bar indicates SD. (H) After treatment of iPSCs-derived or SCs-derived exosomes for 24 h, the percentage of Ki-67-positive cells was shown by flow cytometry analysis to assess the proliferative capacity of SCs. No exosomes treatment served as control group.

presented round membranous vesicle-like structures with an intact plasma membrane. The size of exosomes was relatively uniform and approximately 50–150 nm in diameter. The exosomes contained high electron density substances inside the plasma membrane.

The status of iPSCs-derived exosomes in the suspension was directly and real-timely observed under nanoparticle tracking analyzer. As shown in Fig. 4B, the exosomes were randomly distributed, and each high-bright spot was an exosomal particle. The center of the scattered light spot was the actual position of exosomal particle. In the suspension, each exosomal particle appeared equally likely to move in any direction. Through real-timely tracking the trajectory of each particle, the further motion was totally unrelated to past motion. The motion of particles never stopped. Videos in supporting information (V. S1) reflected the randomly glittering, tumbling motion of iPSCs-derived exosomes. This Brownian motion demonstrated the nanoscale characteristics of iPSCs-derived exosomes. The size of exosomal particles was showed in Fig. 4C. There were two mainly peaks of 105 nm and 165 nm to the size distribution. The mean diameter of iPSCs-derived exosomes was 142.2 ± 64.1 nm. The D50 median diameter was 107.4 nm. The distribution intensity of iPSCs-derived exosomes was showed in Fig. 4D. The width of the distribution (Span) was 1.29. These results indicated that iPSCs-derived exosomes were relatively homogeneous in size.

Supplementary video related to this article can be found at https://doi.org/10.1016/j.bioactmat.2021.12.004

After release from iPSCs, exosomes interacted with recipient cells to influence the biological activity of target cells. During the regeneration of peripheral nerve, axonal growth was mainly supported by SCs, which removed myelin debris and initiated Wallerian degeneration. SCs promotion was interdependent with axonal regeneration through forming bands of Büngner as pathways for outgrowing axons [31]. Therefore, we evaluated the interaction between iPSCs-derived exosomes and SCs to reveal the underlying mechanism of iPSCs-derived exosomes to promote nerve regeneration. Exosomes were tested for their potential to fuse with SCs and deliver their content to the cells. We used blue fluorescent carbon dot-loaded iPSCs to produce exosomes so that the content was labeled with blue fluorescence. Then, iPSCs-derived exosomes were stained with the red membrane fluorescent marker DiI and co-cultured with SCs that were stained with the green membrane fluorescent marker DiO. With the time of co-cultivation, exosomes were gradually internalized by SCs and continuously enriched in the cell cytoplasm (Fig. 4E1). A large number of DiI-positive spots were observed in SCs, and the red fluorescent spots were separated from the green fluorescent cell membrane, indicating that iPSCs-derived exosomes were internalized and localized in cell cytoplasm (Fig. 4E2). Meanwhile, a large number of blue fluorescent spots were also observed in SCs, indicating that exosomes transport these carbon dots from iPSCs to SCs (Fig. 4E3). In the cytoplasm of some SCs, blue and red fluorescence overlapped, indicating that exosomes were endocytosed and still loaded with carbon dots (Fig. 4E4-1, 4-2). In the cytoplasm of other SCs, red fluorescence was on one side of cytoplasm while blue fluorescence was on both sides of cytoplasm, indicating that exosomes released their content after cell endocytosis (Fig. 4E5-1, 5-2). Thus, iPSCs-derived exosomes were endocytosed by SCs in the process of internalization to release their content in the cytoplasm.

Remarkably, after internalization and release of the content, iPSCs-derived exosomes also exhibited an effect on the proliferation of SCs. We compared cell viability and proliferation between iPSCs-derived exosomes treated group and untreated control group through CCK-8 assay. The OD value of optical density represented the number of viable cells. On the first day of co-cultivation, there was no significant difference in the number of proliferative SCs. After 3, 5, and 7 days, the number of viable cells in exosomes treated group was higher than that in untreated control group. There were significant differences between two groups. The proliferative ability of SCs in exosomes treated group was stronger than that in control group, suggesting that iPSCs-derived exosomes could promote cell viability and proliferation of SCs after internalization process (Fig. 4F and G), which could be the underlying mechanism of iPSCs-derived exosomes promoting peripheral nerve regeneration in the following results. Furtherly, we compared SCs proliferative capacity between iPSCs-derived and SCs-derived exosomes through flow cytometry analysis. The percentage of Ki-67-positive cells was 60.0% in iPSCs-derived exosomes group, while it was 46.1% in SCs-derived exosomes group and 42.6% in control group, indicating that the proliferative capacity of SCs was enhanced after treatment with iPSCs-derived exosomes for 24 h. Therefore, the effect of promoting cell proliferation is specifically linked to iPSCs-derived exosomes.

3.4. Construction of acellular nerve grafts with optimized chemical extracted process

ANGs were prepared by using chemical detergents Triton X-200, SB-16 and SB-10. The natural sciatic nerve tissue was milky white in appearance. Under optical microscope there were regular tissue textures in the native nerve (Fig. 5A). After optimized chemical extracted process, the decellularized nerve grafts became soft and uniform while still milky white. No tissue textures were detected in ANGs. To better understand the effect of chemical treatments for decellularization, detailed analyses were performed to examine the efficiency of cellular removal and preservation of the ECM.

The general morphological preservation of chemical treated grafts was assessed under scanning electron microscope. As shown in Fig. 5B, decellularized nerve grafts preserved the three-layer ultrastructure similar to that of native nerve tissue, characterized by epineurium, perineurium, and endoneurium. The integrity of three-dimensional structure was critical for nerve decellularized ECM to promote nerve axon regeneration in vivo. There were irregular collagen fibers on the surface of ANGs, arranged in longitude. These collagen fibers were parallel to the long axis of nerve axons, providing a certain strength for nerve tension. The irregular surface also promoted cell adhesion of surrounding cells, facilitating cell migration and penetration into the inner of ANGs. Moreover, the fibrous mesh-like porous structure was also confirmed inside the ANGs. Porous characteristics guaranteed the diffusion of oxygen and nutrients to support cell migration, propagation and differentiation. Our results showed that ANGs preserved the integrity of three-dimensional structure of native nerve ECM after optimized chemical extracted decellularization.

In addition to the preservation of ECM, all cellular components must be removed including axonal material and Schwann cell material. Myelin protein zero (P0) is the main protein in the myelin structure of peripheral nerve axons. P0 accounts for more than 50% of the total myelin protein, with a molecular weight of 28–30 kDa. As a specific marker protein for SCs, P0 is abundant in natural nerve tissue, as well as the main cause of immune rejection after allogeneic nerve transplantation. We compared the protein distribution of acellular nerve grafts with natural nerve tissue. As shown in Fig. 5C, there were various protein bands with different molecular weights for natural nerve tissue in protein electrophoresis assay. The protein band between 25 kDa and 35 kDa was associated with P0. After chemical decellularization of Triton X-200, SB-16 and SB-10, the P0 protein band disappeared in acellular nerve tissue. The myelin protein components of natural nerve tissue were completely removed after chemical extraction process, resulting in the lower immunogenicity of decellularized allogeneic nerve scaffolds.

To further verify the lower immunogenicity of acellular nerve grafts, immunofluorescence staining was performed between natural nerve and acellular nerve grafts (Fig. 5D). Neurofilament-200 (NF-200) is considered as a specific marker for nerve axons, and S-100 is a specific marker for SCs. In the immunofluorescence staining assay, the protein of NF-200 and S-100 were positively expressed in natural nerve tissue, suggesting that there were antigens of allogeneic nerve axons and SCs while transplanting in vivo. After chemical decellularized treatment with Triton X-200, sulfobetaine-16 and sulfobetaine-10, the acellular nerve

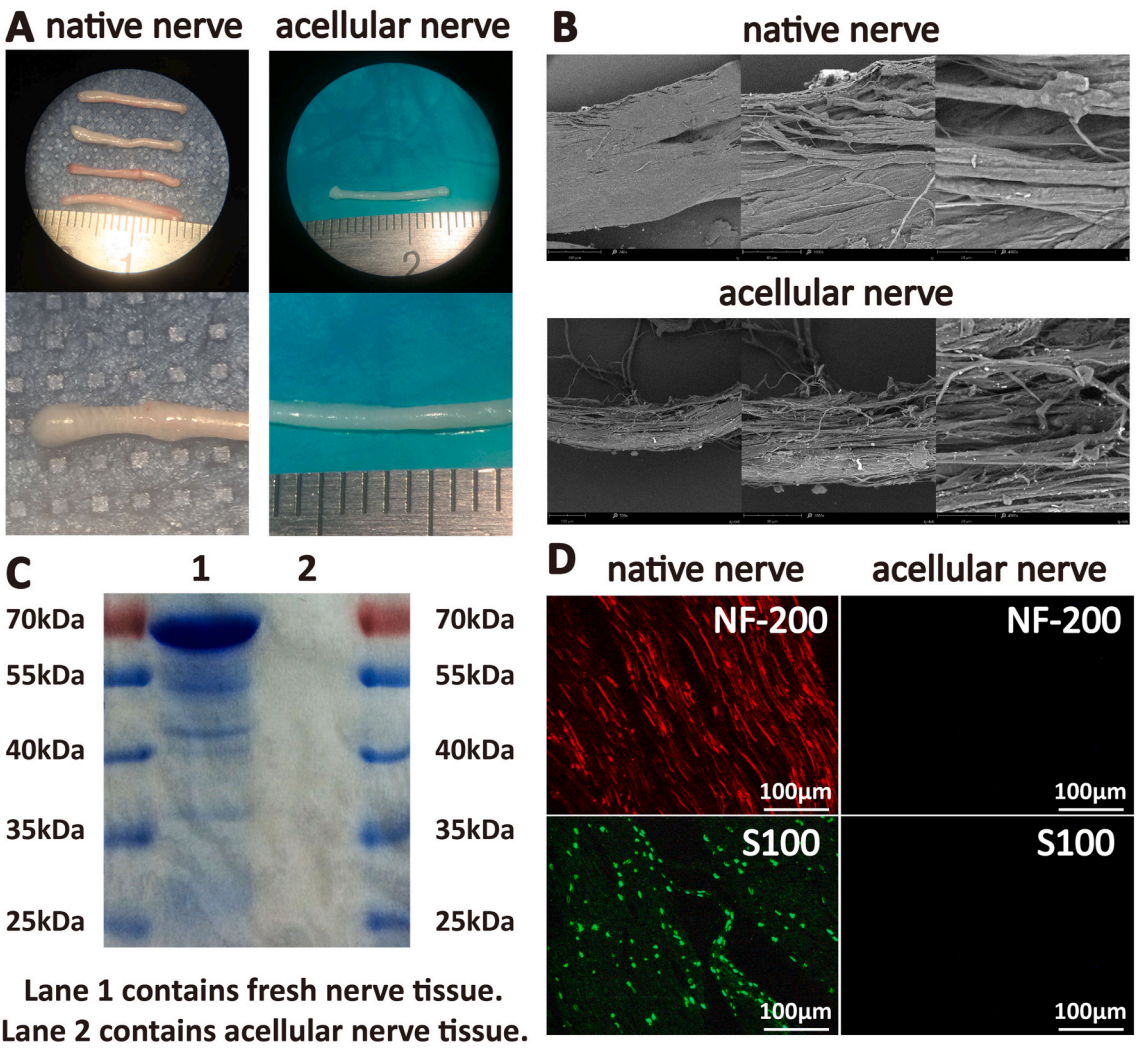

Fig. 5. Characterization of acellular nerve grafts with optimized chemical extracted process. (A) Native sciatic nerve tissue possessed regular tissue textures while acellular nerve grafts had no obvious tissue textures. (B) After chemical decellularization, acellular nerve grafts preserved the integrity of three-dimensional structure through SEM assay. (C) Protein electrophoresis assay of native nerve and acellular nerve grafts. (D) Immunofluorescence staining of native nerve and acellular nerve grafts.

grafts were negative for NF-200 and S100, indicating that the axons, SCs and other antigenic components were completely removed in the acellular nerve grafts. Thus, the prepared decellularized allogeneic nerve grafts can be used for nerve reconstruction in tissue engineering.

3.5. IPSCs-derived exosomes promote motor functional recovery

After preparation of iPSCs-derived exosomes and ANGs, the sciatic nerve was excised in SD rats and the nerve gap of approximately 15 mm was bridged with ANGs combining iPSCs-derived exosomes or not (Fig. 6). Acellular nerve scaffolds provided a natural microenvironment while avoiding the possibility of immune rejection. In rat models of nerve defects, iPSCs-derived exosomes were effective in guiding axonal regeneration and promoting motor functional recovery.

At different time points after restoring the sciatic nerve defect, gait analysis was performed and recorded to calculate SFI (Fig. 7A and B). Motor function was assessed according to SFI, in which 0 corresponded to normal function and −100 corresponded to complete loss of motor function. In the assessment of normal motor function, the values of PLF, TSF, ITF were 0 (Fig. 7C). When the sciatic nerve was severed, the distance between toes decreased and the foot print length increased. Consequently, the values of TSF and ITF were negative, and PLF was positive, resulting in SFI close to −100. At the early stage of 1 and 2 weeks after surgery, there was no significant difference in SFI values among three groups. The SFI values in each group were close to −100. After nerve axonal growth, the rats regained motor function of toe spreading. The SFI value gradually increased with time and approached to 0. At 4, 8, and 12 weeks, the SFI values in the iPSCs-derived exosomes group were significantly higher than those in the ANGs group ($P < 0.05$), suggesting that iPSCs-derived exosomes can promote the recovery of rat motor function (Fig. 7D).

Except for SFI analysis, electrophysiological analysis was also performed to confirm the effect of iPSCs-derived exosomes on motor functional recovery (Fig. 8A). CMAPs are commonly used electrophysiological indexes that reflect the regeneration of nerve axons. After nerve injury, the CMAP latency was prolonged and the maximum amplitude was reduced. At 1 and 2 weeks after operation, no detectable CMAP amplitude was observed in the gastrocnemius and anterior tibialis muscles among three groups, indicating that there was no adequate axon regeneration to restore the continuity of sciatic nerve for impulse conduction. Four weeks later, there were still no CMAPs for gastrocnemius and anterior tibialis muscles in the ANG group. On the contrary, CMAPs of surgical side in the autograft group were detected with weak amplitude, and CMAPs also showed weak amplitude equally in the iPSCs-derived exosomes group. With the regeneration of nerve axons, the continuity of sciatic nerve was restored, resulting in increased amplitude

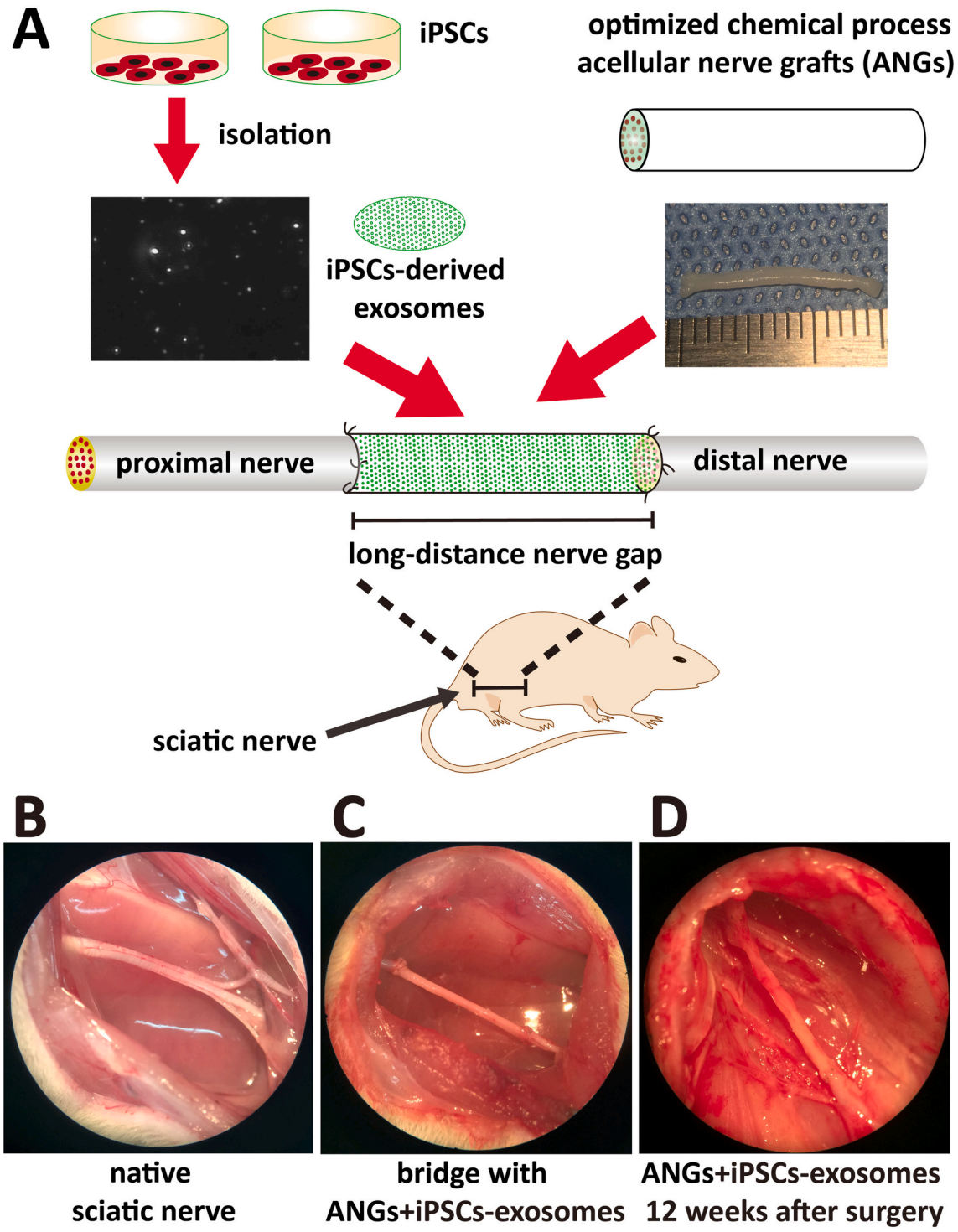

Fig. 6. Acellular nerve grafts and iPSCs-derived exosomes for peripheral nerve regeneration. (A) Schematic outline of cell-free strategy by combining acellular nerve grafts and iPSCs-derived exosomes to promote peripheral nerve regeneration. (B) The natural sciatic nerve and the two terminal branches: tibial nerve and common peroneal nerve. (C) The nerve gap of approximately 15 mm was bridged with ANGs combining iPSCs-derived exosomes. (D) The appearance of ANGs combining iPSCs-derived exosomes 12 weeks after the surgery.

and shortened CMAP latency. At 8 and 12 weeks, CMAP amplitude recovery index of iPSCs-derived exosomes group was significantly higher than that of ANG group. Meanwhile, iPSCs-derived exosomes lowered the CMAP latency of onset. Further analysis showed that iPSCs-derived exosomes also elevated nerve conduction velocity. These results indicate that iPSCs-derived exosomes accelerated axonal regeneration to promote motor functional recovery (Fig. 8B and C).

3.6. *IPSCs-derived exosomes accelerate peripheral nerve regeneration*

The main components of nerve myelin sheath are lipids and proteins, and the structure of myelinated nerve fibers can be displayed by toluidine blue staining. As shown in Fig. 9A–C, nerve myelin sheath was dyed dark blue with toluidine blue, and myelinated nerve fibers presented ring-shaped structure on the cross section. At 12 weeks, the density of

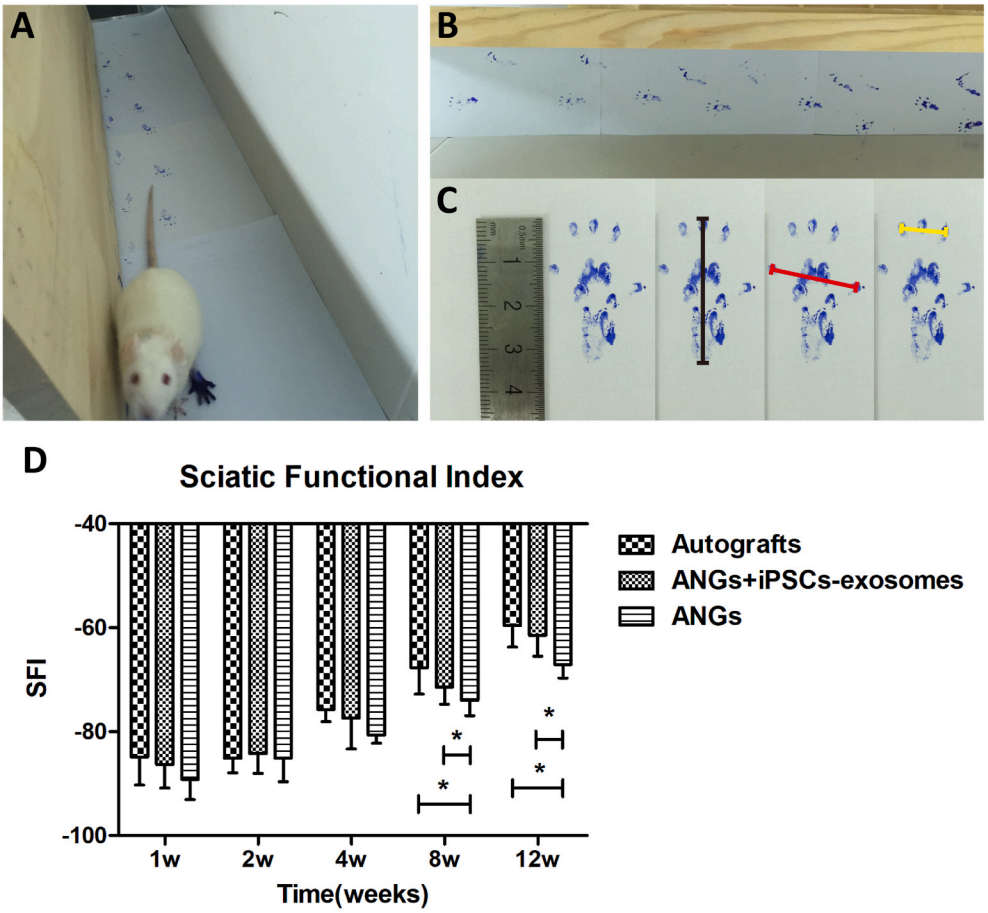

Fig. 7. Motor functional recovery was accelerated after iPSCs-derived exosomes treatment. (A) The rat was allowed to walk down a trace to record their paw prints. (B) The record of walking track. (C) Foot print length, toe spread and intermediate toe spread were measured to calculate sciatic functional index. SFI = 109.5 × TSF +13.3 × ITF -38.3 × PLF - 8.8, where TSF = (ETS-NTS)/NTS, ITF = (EIT-NIT)/NIT, and PLF = (EPL-NPL)/NPL. (D) The SFI in all groups at different time points after surgery. Error bar indicates SD.

myelinated nerve fibers in the autograft group and iPSCs-derived exosomes group were higher than that of allograft group.

Further analysis showed that the cross-sectional area of myelinated axons and the diameter of myelinated axons in the iPSCs-derived exosomes group were significantly higher than those of ANG group at 8 and 12 weeks (Fig. 9D and E). IPSCs-derived exosomes speeded up peripheral nerve regeneration. Compared with the "gold standard" of autografts, iPSCs-derived exosomes increased the number of regenerated myelinated axons, although the diameter and area of myelinated axons were not as good as autografts (Fig. 9F).

3.7. Functional and histological analysis of the reinnervated muscles by regenerative nerve

The two terminal branches of sciatic nerve are tibial nerve to innervate gastrocnemius and common peroneal nerve to innervate anterior tibialis muscle. When sciatic nerve was excised, the continuity of nerve fibers was destroyed to denervate target muscles. The progressive deterioration of motor endplates led to muscle atrophy and weakness. At 1 and 2 weeks after surgery, there were no muscle contraction activity in gastrocnemius and anterior tibialis muscles among all three groups. At 4 weeks, both autograft and iPSCs-derived exosomes groups recovered muscle contraction of gastrocnemius and anterior tibialis muscles other than ANG group. This indicated that the continuity of sciatic nerve was restored ahead to reinnervate target muscles by iPSCs-derived exosomes, which was consistent with the results of electrophysiological analysis. The recovery rate of reinnervated muscle tension by iPSCs-derived exosomes was significantly higher than that treated only with ANGs. At 12 weeks, gastrocnemius and anterior tibialis muscles showed higher muscle maximum tension after treated with iPSCs-derived exosomes (Fig. 10A and B). The reinnervated muscles of iPSCs-derived exosomes exhibited a better motor functional recovery than that of ANGs. Further analysis showed that MTRR of iPSCs-derived exosomes group was also obviously higher than that of ANG group at 8 and 12 weeks postoperatively (Fig. 10C and D). Thus, iPSCs-derived exosomes accelerated the strength recovery of target muscles while accelerating the recovery of nerve conduction in axons.

In addition to muscle strength, muscle mass was also an important index for evaluating nerve regeneration and reinnervation. After surgery, it was observed that gastrocnemius and tibial anterior muscles became smaller and stiffer on the operative side than the normal contralateral side. In order to eliminate the differences of individual weight in experimental animals, the wet weight ratio of target muscles on the surgical side to the contralateral side was calculated to obtain MWMR. As shown in Fig. 10 E and F, the muscle atrophy of gastrocnemius and tibial anterior muscles was identical among all three groups at 1 and 2 weeks postoperatively. There was no significant difference in the MWMR of target muscles between them ($P > 0.05$). At 4 weeks, muscle atrophy was most obvious and all groups showed the lowest MWMR of target muscles. After that, the process of muscle atrophy was terminated and reversed. Compared with allograft group, iPSCs-derived exosomes group showed a higher increase in MWMR of both gastrocnemius and tibial anterior muscles at 8 and 12 weeks. This was attributed to the effect of iPSCs-derived exosomes to promote nerve axonal regeneration. To further compare muscle loss of anterior tibialis muscle and gastrocnemius, we observed that MWMR of tibial anterior muscle in each group was higher than that of gastrocnemius at 8 weeks and 12 weeks ($P < 0.05$). The less muscle loss of anterior tibialis muscle than gastrocnemius was attributed to the thinner diameter of peroneal nerve than tibial nerve. This indicates that in the process of nerve regeneration, nerves with smaller diameters possess a faster recovery than thicker nerves to reinnervate target muscles.

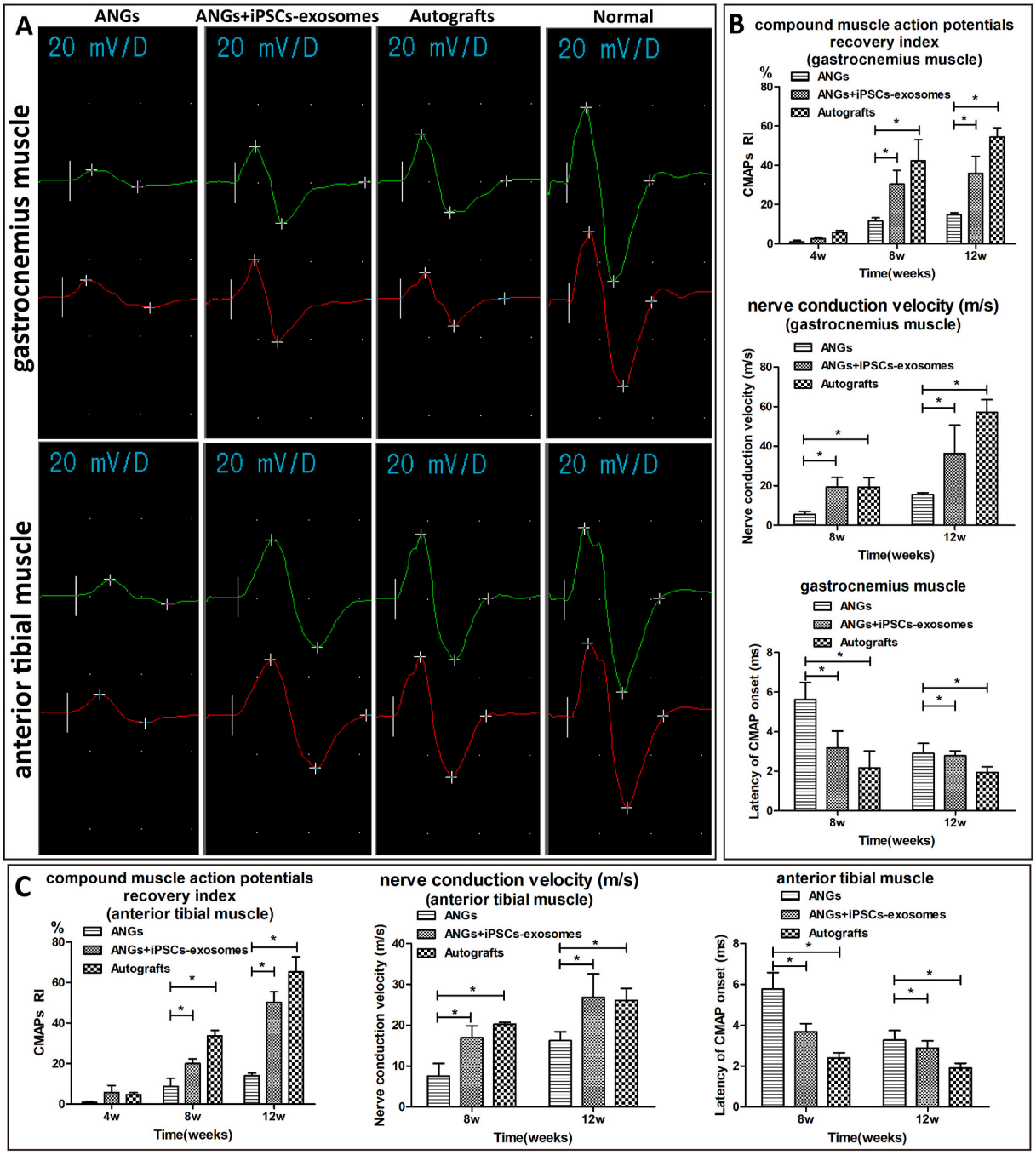

Fig. 8. Electrophysiological measurements were performed at different time points after restoring the sciatic nerve defect. (A) CMAPs for gastrocnemius and anterior tibialis muscles in the ANG group, iPSCs-derived exosomes group, autograft group and contralateral normal nerve group at 12 weeks postoperatively. CMAP amplitude recovery index, nerve conduction velocity, and CMAP onset latency were compared among three groups for gastrocnemius muscle (B) and anterior tibialis muscle (C). Error bar indicates SD.

After nerve injury, gastrocnemius and tibial anterior muscles were denervated to cause the shrinkage of muscle cells. In this case, muscles broke down and were transformed into fat and connective tissue. The histological appearance of target muscles was evaluated at different time points (Figs. S1 and S2). The average diameter and area of muscle fibers were calculated and showed in Fig. 10E and F. At 1 and 2 weeks after surgery, there were no difference in the histological appearance of target muscles among all three groups. The diameter and cross-sectional area of muscle fibers gradually decreased from 1 week to 4 weeks post-operatively. All groups showed the most muscle loss of target muscles at 4 weeks. After that, the diameter and cross-sectional area of muscle fibers was reversed to increase from 4 week to 12 weeks postoperatively. The average diameter and area of muscle fibers in iPSCs-derived exosomes group were significantly higher than that in allograft group at 8 and 12 weeks, indicating that muscle atrophy of gastrocnemius and tibial anterior muscles was reversed by application of iPSCs-derived exosomes. Furthermore, there were no significant difference between iPSCs-derived exosomes and autograft group in the diameter and area of muscle fibers at 8 and 12 weeks. IPSCs-derived exosomes achieved equivalent histological morphology to autografts and thus provided comparable motor functional recovery to autologous nerve transplantation.

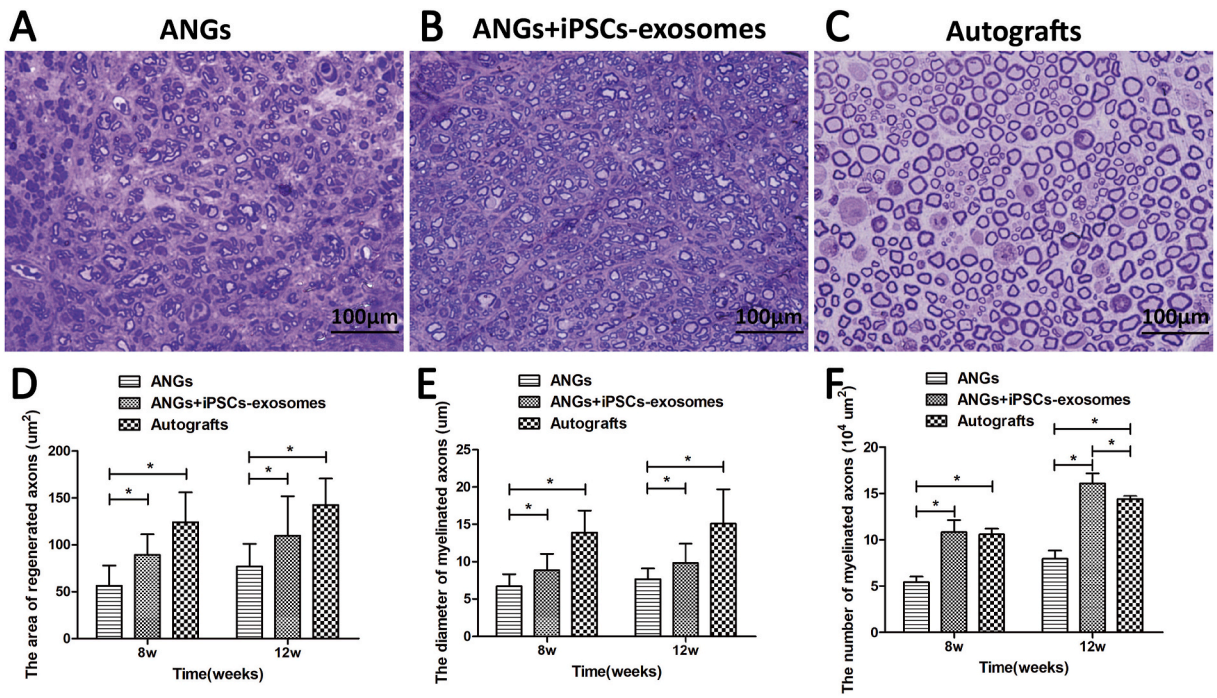

Fig. 9. Toluidine blue staining of regenerated nerve showed regenerated axons in the ANGs group (A), ANGs + iPSCs-derived exosomes group (B) and autograft group (C) at 12 weeks postoperatively. The cross-sectional area of myelinated axons (D), the diameter of myelinated axons (E) and the number of myelinated axons (F) were measured at 8 and 12 weeks after restoring the sciatic nerve defect. Error bar indicates SD. (For interpretation of the references to colour in this figure legend, the reader is referred to the Web version of this article.)

4. Discussion

In this study, we reprogrammed human fibroblasts into iPSCs by introducing four factors of Oct3/4, Sox2, Klf4, and c-Myc. Delivery of the pluripotency-inducing factors could be achieved by using retrovirus, lentivirus, adenovirus [32]. IPSCs generated with retroviral or lentiviral methods tend to result in viral transgene insertions into host genome and their safety is still a concern for clinical applications [33]. Here, Sendai virus vectors, known as cytoplasmic RNA vectors, were used to deliver key genetic factors safely to generate iPSCs free of genomic integration. The obtained human iPSCs were consistent with embryonic stem cells in terms of morphology, proliferation, expression of pluripotent cell-specific markers and surface antigens. The generated iPSCs had the capacity of differentiating into all three germ layers. In proper induction culture, iPSCs differentiated into SCs and mature peripheral neurons, which could enhance peripheral axonal regeneration and myelination.

Despite the promising prospects, the use of iPSCs is still controversial because of their tumorigenic potential. In our study, in vivo teratoma was formed in immunodeficient NOD/SCID mice to confirm pluripotency of iPSCs. Although teratoma is defined as a mixed benign tumor and does not pose a direct risk of forming a malignant tumor, iPSCs may mutate due to certain interactions with their microenvironment, which can lead to uncontrolled cell division. Moreover, iPSCs and their behavior are so complex that the resulting tumors vary greatly in latency, efficiency, and tissue composition. These are closely associated with the number of transplanted cells, injection site, and iPSCs reprogramming methods. Therefore, stem cell-based therapy needs to eliminate the risk of tumorigenesis before clinical applications. With the rise of paracrine hypothesis, exosomes are deemed as a promising alternative to stem cell therapy. Stem cell-derived exosomes are devoid of nuclei and incapable of dividing, making them as a cell-free therapy in the field of regenerative application. We used human iPSCs-derived exosomes to supplement ANGs as a novel strategy to treat long-distance peripheral nerve defects in adult SD rats.

Exosomes are a subtype of extracellular vesicles (EVs) that are released from most eukaryotic cells. EVs are cell-derived vesicles with phospholipid bilayer membrane structure, containing a variety of nucleic acids and soluble proteins. Understanding the exosomal trafficking mechanism will provide insight into how cells employ exosomes for cell-to-cell communication. There are many processes occurred in the signal communication between exosomes and target cells. In this study, we demonstrated that iPSCs-derived exosomes were internalized by SCs through endocytosis to promote cell viability and proliferation. This phenomenon is attributed to the transferred contents of exosomes, in which mRNA can be translated into protein, miRNAs can inhibit the translation of mRNA, and delivered proteins can also affect cellular processes.

After isolation and biological characteristics of iPSCs-derived exosomes, we chose ANGs as tissue engineering scaffolds to bridge long-distance peripheral nerve gaps in rats. Compared with other scaffolds produced from various biological materials, ANGs, also known as decellularized nerve ECM, retain the internal structure and important ECM components of native nerve, such as collagen fibers, laminin and growth factors related to nerve regeneration. The internal three-dimensional architectures include epineurium, perineurium, endoneurium, basal lamina and other microvasculature structures that run longitudinally within the epi- and perineurium to provide blood supply for the endoneurium. Especially for basal lamina, the main component is laminin that guides SCs to arrange and proliferate along basal lamina through mediating cell adhesion. The bands of Bungner are formed to stimulate axon regeneration and reinnervate their end-organ targets. In addition to laminin, other ECM components such as fibronectin and collagen also play an important role in mediating Schwann cell binding and facilitating nerve regeneration.

In this study, we obtained ANGs via optimized chemical extracted process. The components of decellularized ECM were conserved among species and tolerated well by allogeneic recipients. There are physical, chemical and enzymatic treatments or a combination of them to remove all cellular remnants from the tissue [34]. Physical methods disrupt cell membranes, release cell contents, and promote subsequent rinsing of

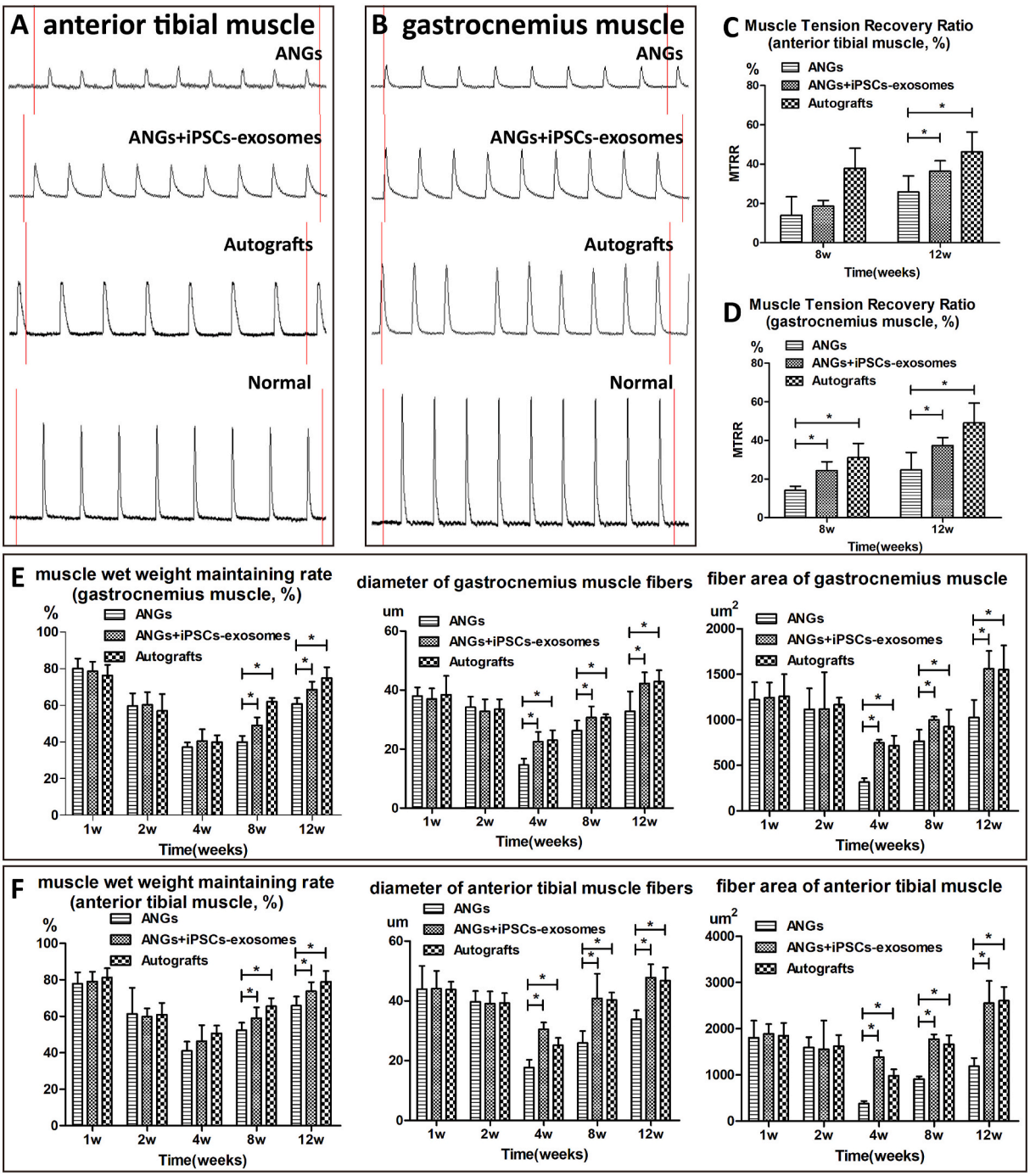

Fig. 10. The functional analysis of target muscles reinnervated by sciatic nerve. (A, B) Muscle strength tests of gastrocnemius and anterior tibialis muscles in the ANGs group, ANGs + iPSCs-derived exosomes group, autograft group and contralateral normal nerve group at 12 weeks postoperatively. (C, D) Muscle maximum tension recovery ratio of gastrocnemius and anterior tibialis muscles at different time points after surgery. (E, F) Muscle recovery measurements of gastrocnemius and anterior tibialis muscles including muscle wet weight maintaining rate, fiber diameter and area of muscle fibers. Error bar indicates SD.

cell contents from the ECM. The physical treatments are usually not enough to achieve complete decellularization. Enzymatic treatments destroy cell membranes and catalyze the hydrolysis of the interior bonds of tissue connections. Complete cell removal by enzymatic treatments entail drawn-out exposure that will destroy ECM structure to further denature laminin, fibronectin, elastin and GAGs in ECM [35]. Chemical extracted treatments can be optimized to completely remove all cellular materials while minimizing any disruption to the three-dimensional architecture of ECM within native tissues. The early protocol for chemically decellularized nerve ECM was created by Sondell et al. through washing the tissue with detergents of sodium deoxycholate and Triton X-100, which demonstrated nerve regeneration successfully without immunological rejection [36]. However, the resulting nerve ECM grafts by Sondell's protocol appeared to fragment the basal laminae. Subsequently, Hudson et al. reported optimized chemical process to engineer an improved acellular nerve graft with intact basal laminae structures similar to native nerve tissue [13]. On the basis of this well preserved basal laminae, we selected Hudson chemical extracted protocol to construct the optimized ANGs. We found that cellular components were completely removed from nerve tissue

including myelin protein, axons and SCs. After decellularization treatment, the three-dimensional architecture of native nerve ECM was preserved in ANGs including epineurium, perineurium, endoneurium and basal lamina. Therefore, ANGs are suitable nerve scaffolds in tissue engineering to support peripheral nerve regeneration.

The traditional ANGs for nerve reconstruction have the limitation of restricted peripheral nerve gap and weak promotion of tissue regrowth. We select iPSCs-derived exosomes to supplement ANGs with the aim of extending the limit distance of peripheral nerves restored by ANGs. At 4 weeks, ANGs failed to repair 15 mm gap of sciatic nerve (no CMAPs and nerve impulse conduction for gastrocnemius and anterior tibialis muscles). After promotion of iPSCs-derived exosomes, nerve axons were regenerated to recover nerve impulse conduction successfully in 15 mm gap of sciatic nerve. IPSCs-derived exosomes are effective to repair long-distance nerve gap bridged by ANGs. Moreover, iPSCs-derived exosomes accelerate motor functional recovery and reverse denervated muscle atrophy. The consequence of denervation is muscle atrophy and functional deficits. Simply restoring nerve impulses but without muscle function, will remain to affect the quality of life seriously.

Functional recovery not only relies on regrowing axons across the gap but also depends on accurate match of motor axons to motor endplates. In the first place, histological analysis was conducted to assess the number of peripheral neurons that had sent axons across the nerve gap and significantly highest number was observed in iPSCs-derived exosomes group among all three groups. This may be due to the trophic effects mediated by iPSCs-derived exosomes to reduce axon apoptosis and boost axon regeneration. Then, the area and diameter of myelinated fibers were used to evaluate the maturation of regenerated fibers. We observed these two parameters in iPSCs-derived exosomes group was significantly higher than ANGs group, though lower than the "gold standard". This is probably associated with the favorable environment created by iPSCs-derived exosomes interaction and their trophic effects. In the second place, the amplitude of CMAP amongst electrophysiological characteristics is related to the number of reinnervated muscle fibers and the value in iPSCs-derived exosomes group was significantly higher than ANGs group. The latency of CMAP reflects the degree of axonal myelination and the latency of iPSCs-derived exosomes was significantly lower than that of ANGs. Nerve conduction velocity is an objective index to evaluate the maturation of regenerated fibers and the NCV value in iPSCs-derived exosomes group was significantly higher than that in ANGs group. These results demonstrate improved muscle reinnervation with the use of iPSCs-derived exosomes. Thirdly, muscle maximum tension correlates with the number of motor units that are recruited when generating the maximum muscle contraction. As expected, we observed higher muscle maximum tension recovery after the action of iPSCs-derived exosomes. Moreover, the fiber diameter and area of muscle fibers were no significantly different as compared with autologous nerve transplantation. In all, we observed better regenerative outcomes achieved with the use of iPSCs-derived exosomes. Although ANGs supplemented with iPSCs-derived exosomes failed to provide equivalent regenerative outcomes to autografts, it certainly exhibited beneficial effects on axonal regeneration and provided comparable motor functional recovery to autologous nerve transplantation.

5. Conclusions

In this study, ANGs supplemented with iPSCs-derived exosomes were used to bridge a 15-mm gap in the sciatic nerve of SD rats. Given the recovery period of 12 weeks, this strategy demonstrated satisfactory regenerative outcomes including axonal growth, reinnervation of target organs and motor functional recovery. This cell-free strategy represents a novel and promising candidate to substitute autologous nerve transplantation in the treatment of long-distance peripheral nerve injury.

CRediT authorship contribution statement

Jianfeng Pan: Conceptualization, Methodology, Formal analysis, Data curation, Writing – original draft. **Meng Zhao:** Methodology, Formal analysis, Data curation. **Xiangjiao Yi:** Methodology, Formal analysis, Data curation. **Jianguo Tao:** Methodology, Formal analysis, Data curation. **Shaobo Li:** Methodology, Formal analysis, Data curation. **Zengxin Jiang:** Methodology, Formal analysis, Data curation. **Biao Cheng:** Conceptualization, Methodology. **Hengfeng Yuan:** Supervision, Writing – review & editing. **Feng Zhang:** Supervision, Writing – review & editing.

Declaration of competing interest

None declared.

Acknowledgements

This study was supported in part by the National Natural Science Foundation of China of China (Contract Grant No. 81702133, 81802144), the Research Project of Shanghai Municipal Health Commission (Contract Grant No. 20194Y0316), and Excellent Youth Training Program of Shanghai Jiaotong University Affiliated Sixth People's Hospital (Contract Grant No. ynyq202102).

Appendix A. Supplementary data

Supplementary data to this article can be found online at https://doi.org/10.1016/j.bioactmat.2021.12.004.

References

[1] M.B. Wilcox, S.G. Laranjeira, T.M. Eriksson, K.R. Jessen, R. Mirsky, T.J. Quick, J. B. Phillips, Characterising cellular and molecular features of human peripheral nerve degeneration, Acta Neuropathol Commun 8 (2020) 51.
[2] A. Faroni, S.A. Mobasseri, P.J. Kingham, A.J. Reid, Peripheral nerve regeneration: experimental strategies and future perspectives, Adv. Drug Deliv. Rev. 82–83 (2015) 160–167.
[3] L. Korus, D.C. Ross, C.D. Doherty, T.A. Miller, Nerve transfers and neurotization in peripheral nerve injury, from surgery to rehabilitation, J. Neurol. Neurosurg. Psychiatry 87 (2016) 188–197.
[4] C.H.E. Ma, T. Omura, E.J. Cobos, A. Latrémolière, N. Ghasemlou, G.J. Brenner, E. Veen, L. Barrett, T. Sawada, F. Gao, G. Coppola, F. Gertler, M. Costigan, D. Geschwind, C.J. Woolf, Accelerating axonal growth promotes motor recovery after peripheral nerve injury in mice, J. Clin. Invest. 121 (2011) 4332–4347.
[5] H. Millesi, Bridging defects: autologous nerve grafts, Acta Neurochir. Suppl. 100 (2007) 37–38.
[6] F. May, A. Buchner, K. Matiasek, B. Schlenker, C. Stief, N. Weidner, Recovery of erectile function comparing autologous nerve grafts, unseeded conduits, Schwann-cell-seeded guidance tubes and GDNF-overexpressing Schwann cell grafts, Dis Model Mech 9 (2016) 1507–1511.
[7] C.A. Holtzer, E. Marani, G.J. Dijk, R.T.W.M. Thomeer, Repair of ventral root avulsion using autologous nerve grafts in cats, J. Peripher. Nerv. Syst. 8 (2003) 17–22.
[8] M. Socolovsky, G.D. Masi, D. Battaglia, Use of long autologous nerve grafts in brachial plexus reconstruction: factors that affect the outcome, Acta Neurochir. 153 (2011) 2231–2240.
[9] C.D. Piao, K. Yang, P. Li, M. Luo, Autologous nerve graft repair of different degrees of sciatic nerve defect: stress and displacement at the anastomosis in a three-dimensional fnite element simulation model, Neural Regen Res 10 (2015) 804–807.
[10] Y. Cho, S. Park, J. Lee, K.J. Yu, Emerging materials and technologies with applications in flexible neural implants: a comprehensive review of current issues with neural devices, Adv. Mater. (2021), e2005786.
[11] C.M. Nichols, M.J. Brenner, I.K. Fox, T.H. Tung, D.A. Hunter, S.R. Rickman, S. E. Mackinnon, Effect of motor versus sensory nerve grafts on peripheral nerve regeneration, Exp. Neurol. 190 (2004) 347–355.
[12] A. Moradzadeh, G.H. Borschel, J.P. Luciano, E.L. Whitlock, A. Hayashi, D. A. Hunter, S.E. Mackinnon, The impact of motor and sensory nerve architecture on nerve regeneration, Exp. Neurol. 212 (2008) 370–376.
[13] T.W. Hudson, S.Y. Liu, C.E. Schmidt, Engineering an improved acellular nerve graft via optimized chemical processing, Tissue Eng. 10 (2004) 1346–1358.
[14] T.W. Hudson, S. Zawko, C. Deister, S. Lundy, C.Y. Hu, K. Lee, C.E. Schmidt, Optimized acellular nerve graft is immunologically tolerated and supports regeneration, Tissue Eng. 10 (2004) 1641–1651.

[15] X. Gu, F. Ding, Y. Yang, J. Liu, Construction of tissue engineered nerve grafts and their application in peripheral nerve regeneration, Prog. Neurobiol. 93 (2011) 204–230.
[16] G. Lundborg, L.B. Dahlin, N. Danielsen, R.H. Gelberman, F.M. Longo, H.C. Powell, S. Varon, Nerve regeneration in silicone chambers - influence of gap length and of distal stump components, Exp. Neurol. 76 (1982) 361–375.
[17] S. Walsh, J. Biernaskie, S.W.P. Kemp, R. Midha, Supplementation of acellular nerve grafts with skin derived precursor cells promotes peripheral nerve regeneration, Neuroscience 164 (2009) 1097–1107.
[18] M. Gnecchi, Z. Zhang, A. Ni, V.J. Dzau, Paracrine mechanisms in adult stem cell signaling and therapy, Circ. Res. 103 (2008) 1204–1219.
[19] B. Bi, R. Schmitt, M. Israilova, H. Nishio, L.G. Cantley, Stromal cells protect against acute tubular injury via an endocrine effect, J. Am. Soc. Nephrol. 18 (2007) 2486–2496.
[20] J. Skog, T. Würdinger, S. Rijn, D.H. Meijer, L. Gainche, M. Sena-Esteves, W. T. Curry Jr., B.S. Carter, A.M. Krichevsky, X.O. Breakefield, Glioblastoma microvesicles transport RNA and proteins that promote tumour growth and provide diagnostic biomarkers, Nat. Cell Biol. 10 (2008) 1470–1476.
[21] H. Valadi, K. Ekström, A. Bossios, M. Sjöstrand, J.J. Lee, J.O. Lötvall, Exosome-mediated transfer of mRNAs and microRNAs is a novel mechanism of genetic exchange between cells, Nat. Cell Biol. 9 (2007) 654–659.
[22] A. Montecalvo, A.T. Larregina, W.J. Shufesky, D.B. Stolz, M.L.G. Sullivan, J. M. Karlsson, C.J. Baty, G.A. Gibson, G. Erdos, Z. Wang, J. Milosevic, O. A. Tkacheva, S.J. Divito, R. Jordan, J. Lyons-Weiler, S.C. Watkins, A.E. Morelli, Mechanism of transfer of functional microRNAs between mouse dendritic cells via exosomes, Blood 119 (2012) 756–766.
[23] W. Stoorvogel, Functional transfer of microRNA by exosomes, Blood 119 (2012) 646–648.
[24] B.W.M. Balkom, O.G. Jong, M. Smits, J. Brummelman, K. Ouden, P.M. Bree, M.A. J. Eijndhoven, D.M. Pegtel, W. Stoorvogel, T. Würdinger, M.C. Verhaar, Endothelial cells require miR-214 to secrete exosomes that suppress senescence and induce angiogenesis in human and mouse endothelial cells, Blood 121 (2013) 3997–4006.
[25] B. Yu, X. Zhang, X. Li, Exosomes derived from mesenchymal stem cells, Int. J. Mol. Sci. 15 (2014) 4142–4157.
[26] L. Sun, R. Xu, X. Sun, Y. Duan, Y. Han, Y. Zhao, H. Qian, W. Zhu, W. Xu, Safety evaluation of exosomes derived from human umbilical cord mesenchymal stromal cell, Cytotherapy 18 (2016) 413–422.
[27] G. Camussi, M.C. Deregibus, S. Bruno, V. Cantaluppi, L. Biancone, Exosomes/microvesicles as a mechanism of cell-to-cell communication, Kidney Int. 78 (2010) 838–848.
[28] K. Takahashi, S. Yamanaka, Induction of pluripotent stem cells from mouse embryonic and adult fibroblast cultures by defined factors, Cell 126 (2006) 663–676.
[29] K. Takahashi, K. Tanabe, M. Ohnuki, M. Narita, T. Ichisaka, K. Tomoda, S. Yamanaka, Induction of pluripotent stem cells from adult human fibroblasts by defined factors, Cell 131 (2007) 861–872.
[30] J. Li, M. Pei, Cell senescence: a challenge in cartilage engineering and regeneration, Tissue Eng. B Rev. 18 (2012) 270–287.
[31] G. Keilhoff, H. Fansa, Mesenchymal stem cells for peripheral nerve regeneration-A real hope or just an empty promise? Exp. Neurol. 232 (2011) 110–113.
[32] I.P. Chen, K. Fukuda, N. Fusaki, A. Iida, M. Hasegawa, A. Lichtler, E. J. Reichenberger, Induced pluripotent stem cell reprogramming by integration-free Sendai virus vectors from peripheral blood of patients with craniometaphyseal dysplasia, Cell. Reprogr. 15 (2013) 503–513.
[33] F. González, S. Boué, J.C.I. Belmonte, Methods for making induced pluripotent stem cells: reprogramming a la carte, Nat. Rev. Genet. 12 (2011) 231–242.
[34] T.W. Gilbert, T.L. Sellaro, S.F. Badylak, Decellularization of tissues and organs, Biomaterials 27 (2006) 3675–3683.
[35] P.M. Crapo, T.W. Gilbert, S.F. Badylak, An overview of tissue and whole organ decellularization processes, Biomaterials 32 (2011) 3233–3243.
[36] O. Frerichs, H. Fansa, C. Schicht, G. Wolf, W. Schneider, G. Keilhoff, Reconstruction of peripheral nerves using acellular nerve grafts with implanted cultured Schwann cells, Microsurgery 22 (2002) 311–315.